The C8-2 '-Deoxyguanosine Adduct of 2-Amino-3-methylimidazo[1,2-d]naphthalene, a Carbocyclic Analogue of the Potent Mutagen 2-Amino-3-methylimidazo[4,5-f]quinoline, Is a Block to R...

ARTICLE *in* CHEMICAL RESEARCH IN TOXICOLOGY · APRIL 2010

Impact Factor: 3.53 · DOI: 10.1021/tx100053n · Source: PubMed

Published in final edited form as:
Chem Res Toxicol. 2010 June 21; 23(6): 1076–1088. doi:10.1021/tx100053n.

The C8-2′-Deoxyguanosine Adduct of 2-Amino-3-methylimidazo[1,2-*d*]naphthalene, a Carbocyclic Analogue of the Potent Mutagen 2-Amino-3-methylimidazo[4,5-*f*]quinoline (IQ), is a Block to Replication in Vitro

Plamen P. Christov[†,1], **Goutam Chowdhury**[§,1], **Craig A. Garmendia**[†], **Feng Wang**[†], **James S. Stover**[†], **C. Eric Elmquist**[†], **Albena Kozekova**[†], **Karen C. Angel**[§], **Robert J. Turesky**[¶], **Michael P. Stone**[†,§,‡], **F. Peter Guengerich**[§,‡], and **Carmelo J. Rizzo**[†,§,‡,*]

[†]Department of Chemistry, Vanderbilt University, Nashville, Tennessee 37235-1822

[§]Department of Biochemistry, Vanderbilt School of Medicine, Vanderbilt University, Nashville, Tennessee 37235-1822

[‡]Center in Molecular Toxicology, Vanderbilt University, Nashville, Tennessee 37235-1822

[¶]Division of Environmental Health Sciences, Wadsworth Center, New York State Department of Health, Albany, NY 12201

Abstract

2-Amino-3-methylimidazo[4,5-*f*]naphthelene is a carbocyclic analogue of the dietary carcinogen 2-amino-3-methylimidazo[4,5-*f*]quinoline (IQ) in which a naphthalene ring system replaces the quinoline unit of IQ. The activity of 2-amino-3-methylimidazo[4,5-*f*]naphthelene (cIQ) in Ames *Salmonella typhimurium* tester strain TA98 is known to be 4-5 orders of magnitude lower than IQ. 2-Amino-3-methylimidazo[4,5-*f*]naphthelene undergoes efficient bioactivation with rat liver microsomes. The C8-dGuo adduct was formed when calf thymus DNA was treated with the *N*-hydroxy-cIQ metabolite and either acetic anhydride or extracts from cells that overexpress *N*-acetyl transferase (NAT). These studies indicate that bioactivation, the stability of the *N*-hydroxylamine ester, and the reactivity of the nitrenium ion with DNA of cIQ are similar to IQ and that none of these factors account for the differences in mutagenic potency of these analogues in Ames assays. Oligonucleotides were synthesized that contain the C8-dGuo adduct of 2-amino-3-methylimidazo[4,5-*f*]naphthelene in the frameshift-prone CG-dinucleotide repeat unit of the *Nar*I recognition sequence. We have examined the in vitro translesion synthesis of this adduct and find it to be a strong replication block to *E. coli* DNA polymerase I, Klenow fragment exo$^-$ (Kf$^-$), *E. coli* DNA polymerase II exo$^-$ (pol II$^-$), and *Sulfolobus solfataricus* P2 DNA polymerase IV (Dpo4). Previous studies by Fuchs and coworkers identified *E. coli* pol II as the polymerase responsible for two-base deletions of the C8-dGuo adduct of *N*-acetyl-2-aminofluorene in the *Nar*I sequence. Our observation that pol II is strongly inhibited by the C8-dGuo adduct of 2-amino-3-methylimidazo[4,5-*f*]naphthelene suggests that one of the other SOS inducible polymerases (*E. coli* pol IV or pol V) is required for its bypass and this accounts for the greatly attenuated mutagenicity in Ames assays compared with IQ.

[*]To whom correspondence should be addressed: Department of Chemistry, Vanderbilt University, VU Station B 351822, Nashville, TN 37235-1822. Phone: 615-322-6100, FAX: 615-343-1234. c.j.rizzo@vanderbilt.edu.
[1]P.P.C. and G.C. contributed equally to this manuscript

Introduction

2-Amino-3-methylimidazo[4,5-*f*]quinoline (IQ, **1**)[2] is a member of a growing family of heterocyclic amines (HCA) that are formed when reducing sugars, amino acids, and creatinine are heated (Maillard reaction); HCAs ared found in all cooked meats (1). IQ is a potent bacterial mutagen and probable human carcinogen (2). The source of its mutagenic and carcinogenic properties lies in its ability to form DNA adducts after appropriate bioactivation (3,4). IQ forms two regioisomeric adducts at the C8- and N^2-positions of dGuo (5). In bacterial assays, IQ was found to be a potent inducer of two-base frameshift deletions in CG-dinucleotide repeat sequences such as that found in the *Nar*I recognition sequence (5′-$G_1G_2CG_3CC$-3′) and the *HisD3052* target sequence (5′-CGCGCGCG-3′) of Ames *Salmonella typhimurium* tester strain TA98 (6).

Subtle structural changes can cause remarkable differences in the bacterial mutagenesis of the HCAs (7,8). For examples, IQ and 2-amino-3-methylimidazo[4,5-*f*]quinoxaline (IQx, **2**) have the same basic molecular skeleton, the only difference being that IQ has a quinoline ring system whereas IQx contains a quinoxaline in which a nitrogen atom replaces the CH at position 9; however, IQx is nearly six-fold less mutagenic than IQ in Ames tester strain TA98, which is designed to detect two-base frameshift deletions (6). Wild and coworkers have examined a series of structural analogues of IQ and found that their mutagenicity in Ames tester strain TA98 varied over one million-fold (Figure 1) (7). The carbocyclic analogue of IQ, 2-amino-3-methylimidazo[4,5-*f*]naphthelene (**3**, cIQ) in which the quinoline unit is replaced by a naphthyl, was found to be nearly five orders of magnitude less potent at inducing two-base deletions than IQ or IQx. These studies also showed that 2-amino-1-methyimidazo[4,5-*f*]quinoline (termed iso-IQ, **4**), which is a regioisomer of IQ, produced

[2]Abbreviations:

IQ	2-Amino-3-methylimidazo[4,5-*f*]quinoline
cIQ	2-amino-3-methylimidazo[4,5-*f*]naphthelene
C8-dGuo-IQ	8-[3-methyl-3H-imidazo[4,5-*f*]quinolin-2-yl)amino]-2′-deoxyguanosine
C8-dGuo-cIQ	8-[3-Methyl-*3H*-naphtho[2,1-*d*]imidazol-2-yl)amino]-2′-deoxyguanosine
Kf	*Escherichia coli* DNA polymerase I, Klenow fragment (“¯ ” denotes exonuclease deficient)
Dpo4	*Sulfolobus solfataricus* P2 DNA polymerase IV
pol II	*Escherichia coli* DNA polymerase II (“¯ ” denotes exonuclease deficient)
ES	electrospray
NAT	*N*-acetyl transferase
DMTr	4,4′-dimethoxytrityl
TIC	total ion current
CID	collision-induced dissociation
BSA	bovine serum albumin
DTT	dithiothreitol
MALDI-TOF	matrix-assisted laser desorption/time-of-flight (MS)
SPE	solid-phase extraction
$Pd_2(dba)_3$	tris(dibenzylideneacetone)dipalladium(0)
XANTPHOS	4,5-Bis(diphenylphosphino)-9,9-dimethylxanthene

two-base deletions nearly eight times more effectively than IQ. Removal of the *N*-methyl group (**5**) significantly reduces the mutagenicity of these analogues in bacteria. The cIQ and iso-IQ analogues have not yet been identified from cooked meats; however, a recent analysis identified iso-IQx and iso-MeIQx as components of cooked meats in concentrations comparable to IQx and MeIQx (9), while N-des-methyl-IQ (**5**) is a metabolite of IQ in mammals (10,11). In related work, Viske and coworkers demonstrated that the mutagenicity of IQ analogues in which the quinoline nitrogen atom was moved from position 6 to positions 7, 8, or 9 were 3-13% that of IQ in TA 98 (8).

The lack of mutagenicity of cIQ (**3**) in Ames assays could be due to low levels of DNA modification resulting from inefficient activation by P450 and/or *N*-acetyl transferase (NAT) enzymes, low reactivity or instability of the activated hydroxylamine ester, or the reduced miscoding properties of the dGuo-cIQ adducts. We have examined the activation of cIQ with rat liver microsomes and the subsequent reactivity of the hydroxylamine ester with calf thymus DNA; DNA modification of cIQ was comparable to that of IQ. In addition, the C8-dGuo adduct of the cIQ (C8-dGuo-cIQ) was incorporated into the frameshift-prone CG-dinucleotide repeat sequence of the *Nar*I recognition sequence and the *in vitro* translesion synthesis by *E. coli* DNA polymerase I, Klenow fragment exo$^-$ (Kf$^-$), *E. coli* DNA polymerase II exo$^-$ (pol II$^-$), and *Sulfolobus solfataricus* P2 DNA polymerase IV (Dpo4) was examined. These study demonstrated that the C8-dGuo-cIQ adduct is a strong block to replication by these polymerases.

Experimental Procedures

All commercially obtained chemicals were used as received. Anhydrous CH_3OH, 1,4-dioxane, and pyridine were also received from Aldrich (Milwaukee, WI) in sure-seal bottles. Toluene was freshly distilled and degassed with argon. CH_2Cl_2 was freshly distilled from calcium hydride. *N,N'*-Diisopropylethylamine was freshly distilled and kept under argon. Melting points are uncorrected. Proton and carbon-13 NMR data were recorded at 400 or 500 MHz and 100 or 125 MHz in solvents as noted. High-resolution FAB mass spectra were obtained from the University of Notre Dame Mass Spectrometry Center (South Bend, IN) using nitrobenzyl alcohol (NBA) as the matrix.

Oxidation of cIQ and IQ by Liver Microsomes from Aroclor-1254 Pre-Treated Rats

Stock solutions (10 mM) of IQ and cIQ were prepared in DMSO. IQ or cIQ (200 μM), EDTA (500 μM), an NADPH-generating system (0.33 mM $NADP^+$, 6.6 mM glucose 6-phosphate, and 1 IU of glucose 6-phosphate dehydrogenase/mL) and microsomes (1 μM P450) from livers of male Sprague-Dawley rats (200-225 g, Charles River Breedeing Laboratory, Wilmington, DE) that were pre-treated with Aroclor 1254 (300 mg/kg, ip, once 3 days before killing), were incubated for 15-30 min at 37 °C in potassium phosphate buffer (100 mM, pH 7.0). The final concentration of DMSO in the reaction mixture was 2% (v/v). The reactions were quenched by adding 1-2 volumes of cold CH_3CN, and the precipitated proteins were removed by centrifugation for 5 min. The supernatant was transferred and the CH_3CN was evaporated under a flow of nitrogen. The aqueous solution containing N-hydroxylated IQ or cIQ was used for either LC/MS analysis or DNA modification.

HPLC and LC-MS/MS^n Analysis of the Oxidation Reactions of cIQ and IQ

The oxidation of IQ or cIQ by rat liver microsomes was analyzed by HPLC with a Hitachi HPLC system and Agilent diode array detector using a C18 column (5 μm, 4.6 mm × 250 mm). LC conditions were as follows: buffer A contained 20 mM $NH_4CH_3CO_2$ (pH 6.8) and 5% CH_3OH (v/v), and buffer B contained 20 mM $NH_4CH_3CO_2$ and 95% CH_3OH (v/v). The

following gradient program was used, with a flow rate of 800 μL min^{-1}: 0-30 min, linear gradient from 95% A (v/v) to 100% B. Peaks were detected at 330 nm.

LC-MS and LC-MS/MS were performed on a Waters Acquity UPLC system and a Waters Synapt hybrid quadropole/OA-TOF mass spectrometer (Waters Corporation, Milford, MA) equipped with a dual chemical ionization/electrospray source (ESCI) source. LC was performed with a Waters Aquity UPLC BEH octadecylsilane column (1.7 μm, 2.1 mm × 100 mm) with the following LC conditions: buffer A contained 20 mM $NH_4CH_3CO_2$ and 5% CH_3OH (v/v), and buffer B contained $NH_4CH_3CO_2$ (20 mM, pH 6.8) and 95% CH_3OH (v/v). The following gradient program (v/v) was used, with a flow rate of 300 μL min^{-1}: 0-7.5 min, linear gradient from 95% A to 100% B; 7.5-8 min, linear gradient to 95% A; 8-10 min, hold at 95% A. The temperature of the column was maintained at 25 °C. Samples (10 μL) were injected with an auto-sampler (Waters Acquity). MS analyses were performed in the positive ionization mode. Electrospray ionization (ESI) conditions were as follows: capillary voltage 2.59 V, sampling cone 30, extraction cone 4.1, source temp 125 °C, desolvation temperature 325 °C, and Trap CE of 6. Acquisition of MS^n spectra was performed with a collision energy of 40. Ion spectra were acquired over the range *m/z* 50-500 using the waters MassLynx V4.1 software.

Reaction of the Microsomal Oxidation Products of cIQ with $K_3Fe(CN)_6$ or NADPH-P450 Reductase

$K_3Fe(CN)_6$ (2 mM) was added to a solution of activated cIQ (50 μL, prepared as described above) and the reaction mixture was incubated at 25 °C for 30 mins. For reaction with reductase, a solution of activated cIQ (50 μL) was incubated with NADPH-P450 reductase (1 μM) and NADPH (1 mM) at 37 °C for 30 min. Following incubation, the reaction mixtures were extracted with ethyl acetate, dried, and dissolved in 9:1 solution of H_2O:CH_3OH (v/v) for LC-MS analysis.

Kinetic Measurements for the *N*-Hydroxylation of IQ and cIQ by Rat Liver Microsomes

The rate of *N*-hydroxylation of IQ and cIQ were determined as previously described (12). Briefly, a solution of liver microsomes (0.4 μM of P450) from rat that had been pre-treated with Aroclor 1254, potassium phosphate buffer (100 mM, pH 7.0), NADPH-generating system (0.33 mM $NADP^+$, 6.6 mM glucose 6-phosphate, and 1 IU of glucose 6-phosphate dehydrogenase/mL) and varying concentrations of IQ or cIQ (0-400 μM) in a total volume of 500 μL were incubated for 10 min at 37 °C. Two volumes of CH_2Cl_2 were added to quench the reactions. The CH_2Cl_2 extracts were removed, evaporated to dryness under a stream of N_2, and dissolved into 400 μL of a solution containing sodium acetate (40 mM) , acetic acid (60 mM), 20% water-saturated amyl acetate (v/v), 4,7-diphenyl-1,10-phenanthroline (1 mM), and $FeCl_3$ (0.4 mM) in ethanol. The color reactions were terminated after incubation for 3 min by adding 20 mM H_3PO_4 (10 μL). Absorbance reading of the solutions was collected at 535 nm and the concentration of *N*-hydroxylated IQ or cIQ were calculated using the extinction coefficient ε_{535} = 39200 M^{-1} cm^{-1} (13). Kinetic parameters were estimated using nonlinear regression analysis using the Graph-Pad Prism software (San Diego, CA).

Reaction of Activated IQ and cIQ with Calf Thymus DNA

A solution of calf thymus DNA (250 μL) was added to a solution of activated IQ and cIQ (250 μL from the preparation described above) so that the final concentration of DNA was 1 mg/mL. The reaction mixtures were briefly vortexed. Acetic anhydride (20 mM) was added and the adduction reaction wa incubated under Ar for 3 h at 37 °C. Following the incubation, the reaction mixtures were extracted with two volumes of $CHCl_3$ and the DNA in the aqueous layer was precipitated with sodium acetate (0.3M, pH 8.0) and cold 70%

ethanol (v/v). The precipitated DNA was washed once with cold 70% ethanol, air-dried, and stored at −70° C.

Reaction of IQ and cIQ with Calf Thymus DNA in the Presence of Rat Liver Microsomes and *S. typhimurium* (strain NW 2009) cell extract

An aqueous solution of IQ and cIQ (200 μM) containing potassium phosphate buffer (50 mM, pH 7.0), EDTA (500 μM), acetylCoA (500 μM), an NADPH-generating system (0.33 mM $NADP^+$, 6.6 mM glucose 6-phosphate and 1 IU of glucose 6-phosphate dehydrogenase/mL), liver microsomes (1 μM P450) from rat pretreated with Aroclor 1254, and *S. typhimurium* (strain NW 2009) cell extract (5 mg/mL total protein) and calf thymus DNA (0.5 mg/mL) were incubated for 3 h at 37 °C. One volume of phenol:chloroform:isoamyl alcohol (25:24:1, v/v/v) was added after the incubution, followed by one volume of $CHCl_3$. The aqueous layer was then dried and stored at −70° C.

Enzymatic digestion

The enzymatic digestion of oligonucleotides was carried out in a single step as follows: calf thymus DNA (0.5 mg) from the adduction reaction was dissolved in Tris-HCl buffer (100 μL, pH 7.05, 50 mM, containing 5 mM $MgCl_2$), DNase I (20 units), alkaline phosphatase (3 units), snake venom phosphodiesterase I type II (0.2 units), and nuclease P1 (4.25 units) were added and the solution was incubated at 37° C for 2 days.

Solid-Phase Extraction of C8-dGuo-IQ and C8-dGuo-cIQ

The enzyme digest samples were purified by SPE using Isolute C18 (EC) 25 mg SPE cartridges. The SPE cartridges were first washed with CH_3OH (1 mL), followed with H_2O (1 mL). The DNA digest samples were loaded in 5% CH_3OH and 0.1% HCO_2H (0.5 mL, v/v). The SPE cartridge was washed with H_2O (1 mL), then 10% CH_3OH (1 mL, v/v). The C8-dGuo-IQ and C8-dGuo-cIQ adducts were eluted with CH_3OH (1 mL). The CH_3OH was evaporated to dryness by vacuum centrifugation, then dissolved in 1:1 CH_3OH/H_2O (80 μL, v/v) for LC-ESI/MS/MS^n analysis.

LC-ESI/MS/MS^n Analyses of the C8-dGuo-IQ and C8-dGuo-cIQ Adducts from the Adduction Calf Thymus DNA

MS analysis was performed in the Vanderbilt University facility on a Finnigan LTQ mass spectrometer (ThermoElectron) equipped with an Ion Max API source and a standard electrospray probe. The sample was introduced with a Waters Acquity UPLC system (Waters, Milford, MA) using an Acquity UPLC BEH Shield RP octadecylsilane column (1.7 μm, 2.1 mm × 50 mm). LC conditions were as follows: buffer A contained 9:1 H_2O/ CH_3CN with 0.1% HCO_2H (v/v) and buffer B contained 100% CH_3CN. The following gradient program (v/v) was used with a flow rate of 200 μL/min: initially 1% B; 4.5 min linear gradient to 20% B; 1 min linear gradient to 100% B; 0.5 min linear gradient 80% B; 0.5 min linear gradient to 10% B; 1 min linear gradient to 1% B; isocratic at 1% B for 2 min. The temperature of the column was maintained at 50 °C and the samples (5 μL) were injected with an auto-sampler (Waters Acquity). The electrospray conditions were as follows: source voltage 2.5 kV, source current 100 μA, N_2 was used as the auxiliary gas at a flow-rate setting of 20, sweep gas flow-rate setting 5, sheath gas flow setting 34, capillary voltage 17 V, capillary temperature 300 °C, and tube lens voltage 65 V. No CID offset was employed. Helium was used as the collision damping gas in the ion trap and was set at a pressure of 1 mTorr. The automatic gain control (AGC) settings in full MS and MS^n were 10000. The MS data were acquired in positive ion mode. The instrument method used for the acquisition of on-line data consisted of a single segment that contained four different scan events. The first and second scan events in the MS/MS scan mode produced the aglycon ion $[BH_2]^+$ adducts

$[M + H - 116]^+$ from the protonated molecules C8-dGuo-IQ ([M + H]+at *m/z* 463), dG-C8-cIQ ([M + H]+ at *m/z* 464) and $^{13}C_{10}$-C8-dGuo-IQ ($[M + H]^+$ at *m/z* 474), under the following conditions (scanning from *m/z* 150 to 800 Da): isolation width 4.0 *m/z*; normalized collision energy 25; activation Q 0.25, and activation time 30 ms. The third and fourth scan events, in the MS^3 scan mode, produced second-generation product ions derived from the aglycon ion adducts $[BH_2]^+$ under the following conditions (scanning from *m/z* 95 to 550 Da): isolation width 2 *m/z*; normalized collision energy 30; activation Q 0.25; activation time 30 ms. One μscan was used for data acquisition and the maximum injection time was 100 ms. The maximum injection time for MS/MS and MS^3 experiments was 50 ms.

Construction of Calibration Curves and Quantitation

External calibration curves were produced in duplicates by the addition of a fixed amount of $^{13}C_{10}$-C8-dGuo-IQ (2.5 pg) as the internal standard, with varying amounts of unlabeled C8-dGuo-IQ (0.6, 2, 2.5, 3.5, 4, 5.5, and 12.3 pg) or C8-dGuo-cIQ adduct (0.6, 1.2, 1.5, 3.3, 5.8, 10.8, and 18.3 pg). The calibration curves were generated in MS/MS scan mode; the transitions for $^{13}C_{10}$-C8-dGuo-IQ, C8-dGuo-IQ and C8-dGuo-cIQ were *m/z* 474 → 353, *m/z* 464 → 348 and 463 → 347, respectively. The calibration curves were plotted as the amount ratio of unlabeled adduct (pg) relative to $^{13}C_{10}$-C8-dGuo-IQ (pg) against the integrated peak area ratio of unlabeled adduct to $^{13}C_{10}$-C8-dGuo-IQ. We have assumed that the ionization efficiency of C8-dGuo-cIQ and C8-dGuo-IQ are comparable. Linear regression was performed using the method of least-squares. The correlation coefficients (r^2) were typically > 0.99. The SPE purified enzyme digest mixture was dissolved in 1:1 CH_3OH/H_2O (80 μL). Aliquots (10 μL) were withdrawn, the internal standard was added (5 pg in 5μL), and injected (7.5 μL) into the UPLC. The level of the corresponding adducts was calculated relative to the amount of DNA in the aliquots and expressed as number of adducts per 10^8 DNA bases.

Chemical Synthesis: 8-[(3-Methyl-*3H*-naphtho[2,1-*d*]imidazol-2-yl)amino]-*N*9-[3′,5′-*O*-(1,1,3,3-tetrakis(isopropyl)-1,3-disiloxanediyl)-β-D-2′-deoxyribofuranosyl]guanine (7)

To a stirred suspension of **6** (100 mg, 0.15 mmol), **3** (43.6 mg, 0.221 mmol), $Pd_2(dba)_3$ (7 mg, 0.0073 mmol), and XANTPHOS (8.5 mg, 0.080 mmol) in anhydrous, degassed toluene (1 mL) under an argon atmosphere, was added lithium bis(trimethylsilyl)amide (1.0 M in THF, 0.29 mL, 0.29 mmol). The reaction was heated to 100 °C and stirred for 30 min, then cooled to room temperature and quenched with saturated $NaHCO_3$ (1 mL). The layers were separated and the aqueous phase was extracted with ethyl acetate. The combined organic extracts were washed with brine, dried over sodium sulfate, filtered and evaporated. Purification by flash chromatography on silica, eluting with 20% ethyl acetate in hexane (v/v), gave an impure mixture of starting material and desired product. Hydrogen gas was bubbled was bubbled through this mixture of products and 10% Pd/C (25 mg, 0.024 mmol) in CH_3OH (10 mL) for 2 h. The mixture was then stirred at room temperature overnight under 1 atm of hydrogen gas. The catalyst was removed by suction filtration and the filtrate evaporated. Purification by flash chromatography on silica, eluting with 2% CH_3OH in CH_2Cl_2 provided **7** (58 mg, 56% overall yield) as a light yellow solid. mp 270–272° C (dec); $[\alpha]^{23}_D$ −36.4° (*c* 0.5, $CH_3OH:CH_2Cl_2$ = 1:1); ^{1}H NMR (DMSO-d_6) δ 10.90 (s, 1H), 8.12 (d, *J* = 8.4, 1H), 7.99 (d, *J* = 8.4, 1H), 7.71 (q, *J* = 13.6, 8.8, 2H), 7.62 (t, *J* = 7.2, 1H), 7.44 (t, *J* = 7.2, 1H), 6.43 (dd, *J* = 13.6, 8.8, 1H), 6.20 (s, 2H), 5.02–4.97 (m, 1H), 3.97–3.96 (m, 1H), 3.89–3.81 (m, 2H), 3.73 (s, 3H), 3.49–3.42 (m, 1H), 2.38–2.31 (m, 1H), 1.08–0.91 (m, 29H); ^{13}C NMR (DMSO-d_6) δ 153.7, 152.8, 152.0, 151.5, 149.9, 148.8, 129.21, 128.7, 127.8, 127.2, 126.2, 123.8, 121.7, 121.1, 120.2, 110.2, 107.4, 84.7, 80.3, 73.9, 64.1, 36.9, 28.2, 17.4, 17.2, 17.2, 17.0, 17.0, 16.9, 12.9, 12.7, 12.4, 12.1; HRMS (FAB NBA) *m/z* calcd for $C_{34}H_{48}N_8O_5Si_2$ (M+H) 705.3364, found 705.3354.

8-[(3-Methyl-*3H*-naphtho[2,1-*d*]imidazol-2-yl)amino]-2′-deoxyguanosine (8)

To a stirred solution of **7** (230 mg, 0.33 mmol) in THF (8 mL) was added tetrabutylammonium fluoride (0.76 mL, 1.0 M in THF, 0.76 mmol). The reaction was stirred at room temperature for 1.5 h after which time the solvent was removed under reduced pressure. Purification by flash chromatography on silica, eluting with 10% CH_3OH in CH_2Cl_2 (v/v), provided **8** (141 mg, 93% yield) as light greenish-gray solid. mp 240–242° C (dec); $[\alpha]^{23}_D$ +53.6° (*c* 0.50, CH_3OH:$CHCl_3$=1:1); ^{1}H NMR (DMSO-d_6) δ 10.88 (br s, 1H), 8.14 (d, *J* = 8.4, 1H), 7.99 (d, *J* = 8.0, 1H), 7.72 (d, *J* = 8.4, 1H), 7.67 (d, *J* = 8.4, 1H), 7.62 (t, *J* = 7.6, 1H), 7.44 (t, *J* = 7.4, 1H), 6.53 (t, *J* = 7.2, 1H), 6.36 (s, 3H), 4.52–4.49 (m, 1H), 3.84–3.80 (m, 1H), 3.72 (s, 3H), 3.69 (d, *J* = 5.2, 1H), 3.55 (dd, *J* = 11.6, 5.6, 1H), 3.36–3.29 (m, 1H), 2.09–2.03 (m, 1H); ^{13}C NMR (DMSO-d_6) δ 153.7, 152.8, 152.2, 150.1, 148.9, 129.2, 128.7, 127.9, 127.5, 126.1, 123.7, 121.6, 121.2, 120.2, 110.1, 107.2, 87.3, 82.0, 71.4, 62.4, 36.1, 28.4; HRMS (FAB, NBA) *m/z* calcd for $C_{22}H_{22}N_8O_4$ (M+H) 463.1842, found 463.1832.

N^2-[(Dimethylamino)methylene]-8-[(3-methyl-*3H*-naphtho[2,1-*d*]imidazol-2-yl)amino]-β-D-2′-deoxyribofuranosyl]guanine (9)

To a stirred solution of **8** (140 mg, 0.303 mmol) in anhydrous CH_3OH (5 mL) under and argon atmosphere was added *N*,*N*-dimethylformamide diethyl acetal (0.4 mL, 2.42 mmol). The reaction was heated to 50 °C and stirred for 2 h. The reaction mixture was allowed to cool to room temperature, upon which time a precipitate formed. The precipitate was collected by suction filtration and washed with cold CH_3OH to afford **9** (130 mg, 83% yield) as a light yellow solid. mp 254–256 °C; $[\alpha]^{23}_D$+20.0° (*c* 0.25, CH_3OH:CH_2Cl_2 = 1:1); ^{1}H NMR (DMSO-d_6) δ 11.52 (br s, 1H), 8.46 (s, 1H), 8.14 (d, *J* = 8.40,1H), 8.00 (d, *J* = 8.00, 1H), 7.75–7.62 (m, 3H), 7.45 (t, *J* = 7.6, 1H), 6.63 (t, *J* = 7.6, 1H), 4.55–4.54 (m, 1H), 3.85–3.82 (m, 1H), 3.72 (s, 3H), 3.69 (d, *J* = 4.40, 1H), 3.57 (dd, *J* = 11.6, 5.2, 1H), 3.30–3.23 (m, 1H), 3.13 (s, 3H), 3.02 (s, 3H), 2.15–2.09 (m, 1H); ^{13}C NMR (DMSO-d_6) δ 157.7, 156.1, 154.8, 151.8, 150.7, 147.5, 129.2, 128.8, 127.8, 126.7, 126.2, 123.8, 121.8, 120.8, 120.22, 111.5, 110.1, 87.2, 82.1, 71.3, 62.3, 40.6, 36.7, 34.5, 28.4; HRMS (FAB NBA) m/z calcd for $C_{25}H_{27}N_9O_4$ (M^+H) 517.2186, found 517.2206.

N^2-[(Dimethylamino)methylene]-8-[(3-methyl-*3H*-naphtho[2,1-*d*]imidazol-2-yl)amino]-*N*9-[5′-*O*-[bis(4-methoxyphenyl)phenylmethyl]]-β-D-2′-deoxyribofuranosyl]guanine (10)

To a stirred solution of **9** (50 mg, 0.097 mmol) in anhydrous pyridine (0.8 mL) and freshly distilled diisopropylethylamine (0.105 mL) under an argon atmosphere, was added 4, 4′-dimethoxytrityl chloride (98 mg, 0.29 mmol) at 0° C. The reaction was warmed to room temperature and stirred for 3 h. The solvent was evaporated, and purification by flash chromatography on silica eluted with 2.0% CH_3OH in CH_2Cl_2 containing 0.5% pyridine (v/v/v) provided **10** (60 mg, 75% yield) as a light yellow solid. mp 212–214° C; $[\alpha]^{23}_D$+11.2° (*c* 0.5, CH_3OH:CH_2Cl_2 = 1:3); ^{1}H NMR (CD_2Cl_2) δ 9.11 (br s, 1H), 8.39 (s, 1H), 8.23 (d, *J* = 7.60, 1H), 7.81 (d, *J* = 8.00, 1H), 7.57 (t, *J* = 7.2, 1H), 7.40 (d, *J* = 7.2, 1H), 7.35 (d, *J* = 7.8, 2H), 7.28 (d, *J* = 8.8, 2H), 7.25–7.21 (m, 4H), 7.13 (t, *J* = 7.6, 2H), 7.05 (t, *J* = 7.2, 1H), 6.68–6.61 (m, 5H), 4.85–4.81 (m, 1H), 4.07 (q, *J* = 11.2, 4.8, 1H), 3.67–3.60 (m, 2H), 3.60 (s, 3H), 3.57 (s, 3H), 3.50 (dd, *J* = 9.6, 6.8, 1H), 3.39 (s, 3H), 3.27 (dd, *J* = 9.6, 4.8, 1H), 3.04 (s, 3H), 2.98 (s, 3H), 2.47–2.41 (m, 1H); ^{13}C NMR (CD_2Cl_2) δ 157.9, 157.8, 157.4, 156.3, 154.7, 151.7, 150.6, 148.3, 147.5, 145.0, 140.2, 135.6, 129.7, 129.6, 129.4, 129.3, 128.9, 128.9, 127.8, 127.6, 127.5, 127.4, 126.4, 124.0, 122.0, 120.8, 120.3, 113.1, 112.9, 112.8, 110.3, 87.3, 85.2, 82.1, 79.9, 71.3, 62.3, 55.0, 54.8, 54.7, 40.7, 36.7, 28.5, 28.4; HRMS (FAB NBA) m/z calcd for $C_{46}H_{45}N_9O_6$ (M+H) 820.3571, found 820.3590.

N^2-[(Dimethylamino)methylene]-8-[(3-methyl-*3H*-naphtho[2,1-*d*]imidazol-2-yl)amino]-*N*9-[5′-*O*-[bis(4-methoxyphenyl)phenylmethyl]-3′-*O*-[[bis(1-methylethylamino](2-cyanoethoxy)phosphino]]-β-D-2′-deoxyribofuranosyl]guanine (11)

To a stirred suspension of **10** (50 mg, 0.061 mmol) and 1*H*-tetrazole (5 mg, .07 mmol) in anhydrous CH_2Cl_2 (3 mL) was added 2-cyanoethyl *N*,*N*,*N*’,*N*’-tetraisopropylphosphorodiamidite (0.028 mL, 0.085 mmol) and stirred for 1.5 h. Purification by flash chromatography on silica, eluting with 2% CH_3OH in CH_2Cl_2 containing 0.5% pyridine (v/v/v), afforded **11** (51 mg, 82% yield) as a light yellow solid. mp 183–185 °C; $[\alpha]^{23}_D$ +102° (*c* 0.5, CH_2Cl_2); ^{1}H NMR (CD_2Cl_2) δ 8.45 (d, *J* = 9.2, 1H), 8.25 (d, *J* = 8.4, 1H), 7.92 (d, *J* = 8.4, 1H), 7.70 (d, *J* = 8.8, 1H), 7.59 (m, 1H), 7.45–7.33 (mm, 4H), 7.27–7.05 (mm, 8H), 6.78–6.61 (mm, 5H), 5.04–4.91 (mm, 1H), 4.21–4.16 (m, 1H), 3.85–3.25 (mm, 18H), 3.05 (s, 3H), 3.01 (s, 3H), 2.57 (t, *J* = 6.2, 1H), 2.46–2.33 (m, 2H), 1.18–1.14 (m, 9H), 1.07 (d, *J* = 8.0 3H); ^{13}C NMR (CD_2Cl_2) δ 158.0, 156.9, 155.1, 154.3, 152.1, 150.9, 148.2, 144.6, 144.6, 144.5, 135.6, 135.4, 129.6, 129.5, 129.4, 129.3, 129.2, 127.9, 127.7, 127.6, 127.2, 127.0, 126.2, 125.9, 124.4, 124.3, 123.5, 121.9, 120.5, 120.0, 117.3, 114.4, 112.4, 108.5, 85.5, 84.1, 81.6, 81.3, 74.7, 74.5, 73.6, 64.1, 63.7, 58.1, 58.0, 57.8, 57.6, 54.6, 54.6, 54.5, 42.9, 42.8, 40.6, 36.0, 35.9, 34.3, 34.1, 31.1, 27.8, 24.8, 24.0, 23.9, 23.8, 23.7, 22.2, 21.7, 19.9, 19.9, 19.8, 19.7; HRMS (FAB NBA) *m/z* calcd for $C_{55}H_{62}N_{11}O_7P$ (M+H) 1019.4571, found 1019.4590.

Oligonucleotide Synthesis

The adducted oligonucleotides were synthesized on an Expedite 8909 DNA synthesizer (PerSeptive Biosystems) on a 1 μmol scale using the UltraMild line of phosphoramidites (phenoxyacetyl-protected dA, 4-isopropyl-phenoxyacetyl-protected dG, acetyl-protected dC, and T phosphoramidites) and solid supports from Glen Research. The manufacturer’s standard synthesis protocol was followed except at the incorporation of the modified phosphoramidites, which was accomplished manually, off-line. At this point, the column was removed from the instrument and sealed with two syringes, one contained 250-300 μL of the manufacturer’s 1*H*-tetrazole activator solution (1.9-4.0% in CH_3CN) and the other contained 250 μL of the phosphoramidite **11** (25 mg, 0.098M in anhydrous CH_2Cl_2). The 1*H*-tetrazole and the phosphoramidite solutions were sequentially drawn through the column (1*H*-tetrazole first), and this procedure was repeated periodically over 30 min. After this time, the column was washed with anhydrous manufacturer’s grade CH_3CN and returned to the instrument for the capping, oxidation, and detritylation steps. The remainder of the synthesis was carried out as normal. The oligonucleotides were purified by HPLC on a C-18 reversed phase column as described below.

5′-CTCGGC-(C8-dGuo-cIQ)-CCATC-3′ (12)

Purified by HPLC using 0.1 M ammonium formate and CH_3OH (v/v) using the following gradient: initially 1% CH_3OH, then a 40 min linear gradient to 50% CH_3OH, isocratic at 50% CH_3OH for 5 min, then a 5 min linear gradient to the initial conditions. 5.2 A_{260} units of oligonucleotide were obtained. MALDI-TOF MS (HPA) *m/z* calcd for (M − H) 3775.58, found 3776.94.

5′-ACTCGGC-(C8-dGuo-cIQ)-CCAATCCTTACGAGCCCCC-3′ (13)

Purified by HPLC using sodium phosphate (pH 7.0, 20 mM) and CH_3OH (v/v) using the following gradient: initially 1% CH_3OH, then a linear gradient to 35% CH_3OH over 27.5 min, a linear gradient to 50% CH_3OH over 2.5 min, isocratic at 50% CH_3OH for 5 min, then a linear gradient to initial conditions over 5 min. MALDI-TOF MS (HPA) *m/z* calcd for (M − H) 8317.6, found 8317.7.

Thermal Melting (T_m) Analysis

The thermal melting analysis of modified duplex (**12**) were performed as previously reported (14).

Optical Spectroscopy

CD and UV spectra of oligonucleotide **12** and its duplex were performed as previously described (14).

NMR Measurements

One- and two-dimensional NMR spectra for C8-dGuo-cIQ-modified 5′-CTCGGC-(C8-dGuo-cIQ)-CCATC-3′ duplex (**12**), were carried out at a ^{1}H NMR frequency of 800 MHz; all spectra were acquired at 15° C. ^{1}H NOESY experiments in D_2O were recorded at mixing times of 250, 200, 150, and 90 ms, with 1024 points in the t1 dimension and 2048 points in the t2 dimension. The relaxation delay was 2s. The data in the t1 dimension were zero-filled to give a matrix of 2K × 2K real points. Magnitude COSY spectra in D_2O were obtained with 16 scans. The data matrix was 256 (t1) × 1024 (t2) complex points. The data in the t1 dimension were zero-filled to give a matrix size of 512 (D1) × 1024 (D2) real points. NOESY spectra for the exchangeable protons were recorded at 5 °C, in 90:10 H_2O:D_2O (v/v), using the Watergate sequence for water suppression and a 250 ms mixing time at a ^{1}H NMR frequency of 600.20 MHz. The NMR data was processed using FELIX (v 97.0, Accelyris, Inc., San Diego, CA) on Silicon Graphics (Mountain View, CA) Octane workstations. Chemical shifts of proton resonances were referenced to the water resonance. Sample preparation for the oligonucleotides was as follows: the modified oligonucleotides were annealed with the complementary d(GATGGCGCCGAG) 12-mer strand at 70 °C with the stoichiometry followed by monitoring single proton resonances in both strands. The resulting 12-mer duplexes were dissolved in 0.250 mL of 10 mM phosphate buffer (pH 7.0) containing 100 mM NaCl and 0.05 mM EDTA in 99.996% D_2O. The oligonucleotide concentrations were determined to be in the region of 0.35-0.7 mM using an extinction coefficient of 1.10×10^5 M^{-1} cm^{-1} at 260 nm (15).

Restrained Molecular Dynamics

Distance restraints and torsion angle restraints were obtained using the same protocol as previously reported (16). Restrained molecular dynamics calculations using a simulated annealing protocol were performed in vacuo using X-PLOR (17). The force field was derived from CHARMM (18) and adapted for restrained molecular dynamics (rMD) calculations of nucleic acids. The empirical energy function consisted of terms for bonds, bond angles, torsion angles, tetrahedral and planar geometry, hydrogen bonding, and nonbonded interactions, including van der Waals and electrostatic forces. Hydrogens were explicitly treated. The van der Waals energy term used the Lennard-Jones potential energy function. The electrostatic term used the Coulomb function, based on a full set of partial charges (-1 per residue) and a distance-dependent dielectric constant of 4*r*. The nonbonded pair list was updated if any atom moved more than 0.5 Å, and the cutoff radius for nonbonded interactions was 11 Å. The effective energy function included terms describing distance and dihedral restraints, in the form of square-well potentials. The rMD calculations were performed in which different starting structures of C8-dGuo-cIQ with the cIQ moiety located in the minor groove (*syn*), major groove (*anti*), and intercalated position (*syn*) were considered. These were generated using INSIGHT II through modification at G7 C8, followed by energy minimization using X-PLOR. Final structures were analyzed using X-PLOR to measure the root-mean-square deviation (rmsd) between an averaged structure and the converged structures.

Oligonucleotide Labeling and Annealing

The labeling and annealing of the oligonucleotides was performed as previously described (19). The concentration of the modified strand was 100 nM.

Single-Nucleotide Incorporation Assays

These assays were performed as previously described with the following modifications (19). The reactions with Kf$^-$ (20), pol II$^-$ (20), and Dpo4 (21) were initiated by the addition of the dNTP with final concentrations of 50, 100, and 250 μM. The polymerase concentration was 48 nM. The Kf$^-$ and pol II$^-$ reactions were run at room temperature for 10 min; the Dpo4 reactions were run at 37 °C for 10 min. The extension reactions with the unmodified template were run under the same reaction conditions except the final concentration of the dNTPs were 1, 2.5, and 5 μM. Reactions were quenched with 70 μL of 20 mM EDTA in 95% formamide (v/v) containing xylene cyanol and bromophenol blue dyes, and heated at 95 °C for 10 min. Aliquots (6 μL) were separated by electrophoresis on a denaturing gel.

Full-Length Polymerase Extension Assays

These assays were performed as previously described with the following modifications (19). The final concentrations of each dNTP were 25, 50, and 100 μM. The polymerase concentration was 48 nM. The Kf$^-$ and pol II$^-$ reactions were run at room temperature for 30 min; the Dpo4 reactions were run at 37 °C for 30 and 60 min. The extension reactions with the unmodified template were run using the same reaction conditions; the concentration of each dNTP was 1, 2.5, and 5 μM. Reactions were quenched by the addition of 70 μL of 20 mM EDTA in 95% formamide (v/v) containing xylene cyanol and bromophenol blue dyes and heated at 95 °C for 10 min. Aliquots (6 μL) were separated by electrophoresis on denaturing gels.

Results

Oxidation of IQ and cIQ by Rat Liver Microsomes

Liver microsomes from Aroclor 1254-treated rats were used for the oxidation of IQ and cIQ and the reaction was monitored by mass spectrometry. The *N*-hydroxylated IQ derivative has been previously characterized and the mass spectrum of the metabolite obtained from our preparation matched that which was reported (22). Hydroxylation of the cIQ resulted in two products with *m/z* 214.1, consistent with the desired product (Figure 2, panels A). The MS/MS spectrum of the major oxidation product (Figure 2, Panel B, bottom) possessed fragment ions at *m/z* 182.1 consistent with the loss of NHOH (32 Da); this fragmentation was not observed for the minor product and is consistent with the major product being the *N*-hydroxylamine (23-25). The *N*- versus ring hydroxylation products was also differentiated chemically. The major product was completely consumed when treated with $K_3Fe(CN)_6$ (Figure 2, Panel C); presumably the aryl nitroso or nitro species were the product of this reaction although they was not observed. The minor product did not react with $K_3Fe(CN)_6$. Additionally, the oxidation products were treated with NADPH and NADPH-P450 reductase resulting in partial reduction of the major product (Figure 2, panel C), while minor product was not reduced under these conditions. Finally, the microsomal oxidation reaction resulted in a positive colorometric assay for *N*-hydroxylamines when treated with Fe^{3+} and 4,7-diphenyl-1,10-phenanthroline indicator (12,13,26). These observations are consistent with *N*-hydroxylation being the major biotransformaion pathway product by microsomal oxidation of cIQ. Rates of IQ and cIQ hydroxylation by the rat liver microsomes were measured using a previously established assay (12). Steady-state kinetic analysis revealed that the hydroxylation efficiencies (k_{cat}/K_m) for IQ and cIQ were nearly identical (Figure 3).

Activation of IQ and cIQ and Modification of Calf Thymus DNA

An equimolar mixture of IQ (**1**) and cIQ (**3**) was *N*-hydroxylated by the rat liver microsomal preparation, and then activated further with either acetic anhydride or cell extracts of bacteria over-expressing NAT enzyme supplemented with acetylCoA, in the presence of calf thymus DNA. With authentic standards in hand (*vide infra*), the C8-dGuo-IQ and C8-dGuo-cIQ nucleosides were identified (Figure 4), from the modified calf thymus DNA by LC-ESI/MS/MS^n. The two modified nucleosides were readily separated by UPLC (Figure 5, panel A). The masses of the C8-dGuo-IQ (*m/z* 464.2) and C8-dGuo-cIQ (*m/z* 463.2) nucleosides differ by only 1 Da. Both nucleoside adducts undergo fragmentation at the MS/MS scan stage to produce the aglycon adducts $[BH_2]^+$ attributed to the loss of the deoxyribose unit (-116 Da) (C8-dGuo-IQ *m/z* 348.5 and C8-dGuo-cIQ 347.3). The MS^3 product ion spectrum acquired on the *m/z* 348.5 ion from C8-dGuo-IQ $[M+H-dR]^+$ was identical to the standard and to that reported previously (Figure 9, panel B) (27,28). The product ion spectrum obtained from the *m/z* 347.3 ion of the C8-dGuo-cIQ $[M+H-dR]^+$ gave a similar fragmentation pattern and was also identical to the standard (Figure 5 panel C). Prominent fragment ions are observed at *m/z* 331 and 303 for dG-C8-IQ, and *m/z* at 330 and 304 for dG-C8-cIQ, fragment ions that are consistent with the loss of NH_3 and $CONH_3$ from guanine. The N^2-dGuo adducts were not detected.

The formation of the C8-dGuo-IQ and C8-dGuo-cIQ adducts in calf thymus DNA was quantified using a $^{13}C_{10}$-labeled C8-dGuo-IQ nucleoside as an internal standard (Figure 5, panel D). A calibration curve (r^2 0.99) was developed by plotting the concentration of C8-dGuo-IQ (0.6 – 12.3 pg) / $^{13}C_{10}$-C8-dGuo-IQ (2.5 pg) versus the integrated ratio of C8-dGuo-IQ (*m/z* 464 → 348) / $^{13}C_{10}$-C8-dGuo-IQ (*m/z* 474 → 353); the calibration curve for the C8-dGuo-cIQ adduct (0.6 – 18.3 pg; *m/z* 463 → 347) and the $^{13}C_{10}$-C8-dGuo-IQ standard was developed in a similar fashion (r^2 0.99) (see Figure S1 of the Supporting Information for calibration curves). We observed that activation of the *N*-hydroxylamines with acetic anhydride gave higher levels of the C8-dGuo adducts than with acetylCoA and NAT from bacterial extracts (Table 1). In both cases, we observed that the C8-dGuo-cIQ level was slightly higher than the C8-dGuo-IQ. Collectively, these data suggest that neither differential bioactivation, nor the stability or reactivity of the corresponding nitrenium ions account for the dramatically different mutagenicity of IQ and cIQ.

Synthesis of the Modified Nucleoside and Oligonucleotides

2-Amino-3-methylimidazo-[4,5-*f*]naphthelene (**3**) was prepared according to Kaiser *et al.* starting from 1-nitroso-2-naphthol (7,29). The phosphoramidite reagent of the C8-dGuo-cIQ adduct was synthesized by a route analogous to that described earlier for the C8-dGuo-IQ adduct (Scheme 1) (14). Buchwald-Hartwig coupling of protected 8-bromo-dGuo derivative **6** with **3** was accomplished using XANTPHOS as the ligand for Pd(0) (30,31). Purification of the coupling product was best accomplished after hydrogenolysis of the O^6-benzyl protecting group affording **7** in 59% yield for the two steps. Deprotection of **7** with fluoride provided the modified nucleoside **8** in 93% yield. The modified nucleoside was then converted to the corresponding protected phosphoramidite reagent **11** in three steps (14).

Two oligonucleotide sequences were synthesized in which the C8-dGuo-cIQ adduct was incorporated at the frameshift-prone G_3-position of *Nar*I recognition sequence (32,33). A manual coupling protocol was used for the incorporation of the modified nucleotide and the oligonucleotides were characterized by MALDI-TOF-MS analysis (14). The first oligonucleotide was a 12-mer sequence 5′-CTC*G*$_1$*G*$_2$*C*$\underline{\boldsymbol{G}}_3$*CC*ATC-3′ (**12**) where $\underline{\boldsymbol{G}}_3$ is the modified nucleotide and the *Nar*I recognition sequence is in italic. The thermal melting temperature (T_m) of the duplex containing **12** was 61° C, 4° C lower than the unmodified duplex. This value is the same as the C8-dGuo-IQ adduct in the same sequence context

(14,34). NMR studies confirmed that the C8-dGuo-IQ adduct adopts a base-displaced intercalated conformation in which the modified guanine possesses a *syn* glycosidic geometry and the modified G-C base pair is displaced into the major groove (16).

Preliminary conformational assignments of the C8-dGuo-IQ adduct were previously based on UV and CD spectral analysis (14,34). Cho and coworkers have correlated the conformation of the C8-dGuo adducts of 2-aminoflourene (AF) with the sign of the induced CD of the AF chromophore (35). A positive induced CD was indicative of a *syn* glycosidic geometry of the modified base and a base-displaced intercalated or minor groove-bound conformation. Alternatively, a negative induced CD was observed when the AF-adduct was bound in the major groove with an *anti* geometry about the glycosidic bond. We applied this analysis to the C8-dGuo-IQ adducts, which showed a positive induced CD of the IQ chromophore (34). The base-displaced intercalated and minor groove-bound conformations were differentiated by their UV spectra; a perturbation in the IQ chromophore was observed for the base-displaced intercalated conformation but not when the adduct was positioned in the minor groove. The induced CD of the C8-dGuo-cIQ adduct in duplex **12** is positive suggesting a *syn* glycosidic geometry and either a base-displaced intercalated or minor groove-bound conformation (Figure 6). The UV spectrum showed no perturbation of the long-wavelength absorbance assigned to the 2-amino-3-methyl-imidazo[4,5-*f*]naphthelene ring system consistent with a minor groove-bound conformation. However, the UV spectrum strongly resembles that of C8-dGuo-AF adduct in the same sequence, which did not show a perturbation of the AF chromophore even though NMR studies revealed the adduct to be ~50% intercalated (34).

NMR Analysis of C8-dGuo-cIQ containing Duplex 12

In addition to UV and CD spectroscopy, we utilized chemical shift analysis of the adduct protons and NOESY to determine the conformation of the C8-dGuo-IQ adduct in the *Nar*I sequence. The chemical shifts for the IQ protons were the most upfield when the C8-dGuo-IQ adduct adopted a base-displaced intercalated conformation. All of the IQ protons for this duplex were shifted upfield by up to 0.4 ppm relative to the chemical shift of the nucleoside. In the present case, the cIQ protons of the duplex containing **12** were shifted upfield by 0.6-1.1 ppm relative to the nucleoside (Table 2, using the numbering system for IQ followed by an A to distinguish from the nucleobase numbering; see Figure 4), suggesting that the C8-dGuo-cIQ adduct of duplex **12** adopts a base-displaced intercalated conformation. NOESY spectra confirmed this assignment but suggested an alternative orientation of the cIQ group from that of IQ.

The adduct protons were assigned from a combination of 1D, NOESY and COSY spectra (Figure S4 of the Supporting Information). Nineteen NOEs were observed between the cIQ moiety and the DNA protons (Figure 7 and Figure S2, S3, and S5 in the Supporting Information). The observed NOEs between $\underline{G}^{7}$ H1′→cIQ CH_3 and C^{8} H1′→cIQ CH_3 (Figure S3 in the Supporting Information) indicated that the cIQ N3-methyl group is oriented in the minor groove (see Figure 8 for residue numbering), orienting the cIQ H4A, H5A and H6A protons facing into the minor groove, and the cIQ H7A, H8A, and H9A protons facing into the major groove. The cIQ H4A proton exhibited an NOE to G^{19} H1′. The cIQ H5A proton exhibited NOEs to G^{19} H1′, H4′, H5′ and H5″, G^{17} H1′, and C^{18} H1′. The cIQ H6A proton exhibited NOEs to G17 H2′ and H2″, and C18 H2′. NOEs were observed between cIQ H7A and G17 H8, H1′, H2′ and H2″, and C18 H1′. The cIQ methyl protons also exhibited NOEs to G^{17}N1H, and G^{19} N1H (Figure S3 in Supporting Information). The observed NOEs are consistent with cIQ moiety in the intercalated position and the N3-methyl group oriented toward the minor groove.

Figure 8 shows a plot of the change in chemical shift (Δδ) of the base aromatic protons (A) and the ribose anomeric protons (B) versus those of the unmodified duplex. As expected, the largest perturbations are observed with the nucleotide pairs flanking the modification site. A significant upfield chemical shift change was observed for the Gua that is complementary to the Cyt on the 3′-side of the adduct (Figure 5, position G17). This chemical shift change is ~ 0.3 ppm larger than that seen for the C8-dGuo-IQ adduct in the same sequence. All other chemical shift changes are similar to that of the C8-dGuo-IQ modified duplex.

In vitro Translesion Synthesis

A modified 27-mer oligonucleotide containing the *Nar*I recognition sequence was used for *in vitro* replication studies (**13**, see Figure 9 for the sequence). The C8-dGuo-cIQ adduct was incorporated at position 8 of the modified 27-mer (**13**) and annealed to a 5′-^{32}P-labeled 19-mer, −1 primer strand for single nucleotide incorporation studies. Kf^{-} and Dpo4 inserted only dCTP opposite the C8-dGuo-cIQ adduct (Figures S7 and S9 of the Supporting Information); the insertion efficiency for Kf^{-} was low and incorporation was only observed at the highest dCTP concentration. Insertion of dGTP and dCTP opposite the modification was observed for pol II^{-} (Figures S8 of the Supporting Information). A small amount of a second insertion was observed at the highest dCTP concentration, which is consistent with a two-base deletion in this sequence context. All three polymerases inserted only dCTP when an unmodified template was used. The dNTP selectivity opposite the C8-dGuo-cIQ adduct parallels that of the C8-dGuo-IQ adduct in the same sequence context, although the insertion efficiencies appeared to be lower (19).

The modified 27-mer **13** (***G*$_3$** is C8-dGuo-cIQ) was then annealed to a 5′-^{32}P-labeled 16-mer, −3 primer strand to examine the ability of the polymerases to bypass and extend past the C8-dGuo cIQ adduct in the presence of all four dNTPs (Figure 9). The C8-dGuo-cIQ adduct was a strong block to all three polymerases. In each case, extension was blocked one base prior to the adduct site, indicating that insertion of a dNTP opposite the adduct was strongly inhibited. Low levels of insertion opposite the adduct was observed for Kf^{-} and pol II^{-}; however, further extension was blocked. Insertion opposite the adduct was most efficient for Dpo4. If the extension reaction was run for a longer time (60 min), very low levels of full-length extension products were observed for the Dpo4 (gels not shown). Full extension of the unmodified template was observed for all three polymerases (***G*$_3$** is dGuo).

Discussion

Arylamines require metabolic activation in order to modify DNA. The initial step is a P450 *N*-hydroxylation; the primary enzyme that metabolizes IQ and related heterocyclic amines are P450 1A2 and 1A1 (12). The *N*-hydroxylamine is then esterified by NAT to its *N*-acetoxy derivatives; the hydroxylamine ester undergoes solvolysis to the corresponding aryl nitrenium ion, which is the DNA modifying species. A comparative study showed that *N*-hydroxylation of 4-aminobiphenyl (ABP), IQ, 2-amino-3-methylimidazo[4,5-*f*]quinoxaline (MeIQx), 2-amino-1-methyl-6-phenyl[4,5-*b*]pyridine (PhIP), and 2-amino-5-methyldipyrido[1,2-*a*:3′,2′-*d*]imidazole (Glu-P-1) by human liver microsomes only differed by ~2-fold over this series of structurally diverse substrates (36). A ten-fold difference in catalytic efficiency was observed for these substrates with rat P450 1A2; in this case Glu-P-1 was the best substrate while 2-amino-3,4-dimethylimidazo[4,5-*f*]quinoline (MeIQ) was the worse (26). A related study reported that the *N*-hydroxylation of PhIP and MeIQx by human microsomes or recombinant human P450 1A2 were similar (37). The rates of *N*-acetylation of *N*-hydroxy-ABP and *N*-hydroxy-AF by human liver cytosol were significantly higher than for the *N*-hydroxy derivatives of the heterocyclic amines IQ, MeIQx, PhIP, and Glu-P-1 (36). The *N*-hydroxylation of IQ, PhIP, and 3-amino-1-methyl-*5H*-pyrido[4,3-*b*]indole (Trp-P-2) by recombinant human and rat P450 1A1 have also been examined (38).

The efficiency (V_{max} / K_m) for the *N*-hydroxylation differed by 63- and 15-fold for the human and rat enzymes, respectively, with PhIP being the best substrate and IQ the worse for both enzymes. Differences in the rate of N-O bond heterolysis to generate the DNA modify nitrenium ion and the reactivity of the nitrenium ion can also influence the level of DNA adducts (39).

We examined the activation of IQ and cIQ by rat liver microsomes, the conversion of the corresponding hydroxylamines to their *N*-acetoxy derivatives by acetylCoA and NAT or acetic anhydride, and measured the levels of C8-dGuo adducts from the reaction of the activated substrates with calf thymus DNA. Mass spectrometry was used to quantitate the adducts, and we observed that the levels of C8-dGuo-cIQ were slightly higher than the levels of the C8-dGuo-IQ adduct. This analysis assumed that the ionization efficiency of C8-dGuo-cIQ and C8-dGuo-IQ are comparable. While the ionization efficiency of the modified nucleosides may differ slightly, the difference is not expected to significantly change the relative quantitation of the adducts compared to the difference in mutagenicity. The data suggests that the two-stage activation of cIQ, the solvolysis to the nitrenium ion, and reactivity with guanine bases do not explain its low mutagenicity in Ames assays compared to IQ.

The C8-dGuo adducts of the simple arylamines 2-aminoflourene (AF) and *N*-acetyl-2-aminoflourene have been extensively studied in the *Nar*I recognition sequence (Figure 2). This sequence contains a CG-dinucleotide repeat unit and is a hot spot for arylamine-induced two-base deletions (32,33,40). Bacterial mutagenesis using site-specifically modified oligonucleotides demonstrated that two-base deletions were the predominant mutational event only when the C8-dGuo-AAF adduct was situated at the G_3-position of the *Nar*I sequence. Modification of the G_1- and G_2-positions resulted in largely G → T transversions.

Using in vitro and in vivo methods, Fuchs and coworkers determined that the SOS inducible polymerases II, IV, and V have specific roles in the error-prone and error-free bypass of the C8-dGuo-AAF adduct. Replication of the C8-dGuo-AAF adduct at the G_3-position of the *Nar*I sequence by pol II results in two-base deletions while pols IV and V result in base-pair substitution and error-free bypass, respectively. In vitro studies showed that pol II also produce nearly equal amounts of the one-base deletion product, which are not observed in vivo (41). While the C8-dGuo-AAF adduct is a block to pol III, the presence of pol III suppressed the one-base deletion product. The β-clamp and RPA accessory proteins also play an important role in the bypass (42). Replication of the C8-dGuo-AAF adduct in this sequence by Kf also produces two-base deletions in vitro (43). Although structurally related to AAF, the C8-dGuo-AF only gave low levels of two-base deletions when placed in the frameshift-prone position of the *Nar*I sequence (44).

The marked differences in mutagenicity in the Ames tester strain *S. typhimurium* TA98 in response to modest structural changes (Table 1) make IQ and it structural analogues an ideal system to study structure-activity relationships of arylamine mutagenesis. We have previously examined the *in vitro* replication of the C8- and N^2-dGuo adducts of IQ in the frameshift prone G_3-position of the *Nar*I recognition sequence (19,45). Replication of the C8-dGuo-IQ adduct by Kf^-, pol II^-, and Dpo4 resulted in two-base deletions. A one-base deletion product was also observed with pol II^- in approximately equal amounts as the two-base deletion product (19,45). Pol II^- bypassed and extended the C8-dGuo-IQ adduct most efficiently, whereas Kf^- was the least efficient. In the present study, we examined the in vitro replication of the C8-dGuo adduct of 2-amino-3-methylimidazo-[4,5-*f*]naphthelene (cIQ, **3**), a closely related structural analogue of IQ in which the quinoline nitrogen atom is replaced by a CH. In contrast to the C8-dGuo-IQ and C8-dGuo-AAF adducts, in vitro

replication of the C8-dGuo-cIQ adduct in sequence **13** by Kf^{-}, pol II^{-}, and Dpo4 did not result in two-base deletions; in fact, the C8-dGuo-cIQ appears to be a strong replication block to these polymerases.

Structural studies using multi-dimensional NMR and restrained molecular dynamics calculations of duplexes containing the C8-dGuo adducts of AF, AAF, and IQ in the *Nar*I sequence have been reported (46-49). The C8-dGuo-AF adduct was found to be in conformational exchange between the base-displaced intercalated and major groove-bound conformations, with the position of the equilibrium dependent of the local sequence. We have reported the conformation of the C8-dGuo-IQ adduct at all three dGuo positions of the *Nar*I sequence and find this adduct to be conformationally distinct from C8-dGuo-AF. We observed a single conformation for the C8-dGuo-IQ modified duplexes. The base-displaced intercalated conformation was observed when the C8-dGuo-IQ adduct was placed at the G_3-position, while a minor-groove-bound conformation was observed for the G_1- and G_2-modified duplex (16,34,50).

Preliminary spectroscopic studies (CD, UV, chemical shift analysis, and NOESY) suggest that the C8-dGuo-cIQ adduct adopts a base-displaced-intercalated conformation when situated at the G_3-position of the *Nar*I sequence (**12**); no exchange cross-peaks were observed suggesting a single conformation. Interestingly, average refined structure revealed that the orientation of the cIQ adduct relative to the helical axis differs from that of the C8-dGuo-IQ modified duplex (Figure 10) (16). The N3-methyl group of the C8-dGuo-IQ protruded into the major grove, whereas the N3-methyl of the C8-dGuo-cIQ adduct is exposed to the minor groove. In this regard, the adduct orientation is more similar to the C8-dGuo-IQ when situated at the G_1- and G_2-positions (50). Many DNA polymerases make contact with the duplex in the minor groove and the orientation of the N3-methyl group may contribute to the blocking nature of this adduct. The cIQ moiety is well stacked and nearly parallel to the neighboring base pairs. This is in contrast to the C8-IQ adduct in which the IQ group is stacked but canted at a 23° angle. The comparison of the chemical shifts of the anomeric and base protons between the C8-dGuo-cIQ modified and unmodified duplexes reveal a large downfield chemical shift for the protons resonances of the neighboring $C^6{\cdot}G^{19}$ base pair to the 3′-side of the adduct. The magnitude of the chemical shift change for the dGuo of the complementary strand is ~0.3 ppm larger than for the duplex containing the C8-dGuo-IQ adduct (16). This chemical shift difference may be reflective of the better stacking arrangement of the cIQ with the $C^6{\cdot}G^{19}$ base pair (also see Figure S6 of the Supporting Information) compared to that of the IQ moiety in the identical sequence context. However, the $C^8{\cdot}G^{17}$ base pair on the 5′-side of the C8-dGuo-cIQ adduct is perturbed, and this misalignment might contribute to the inhibition of the extension step during lesion bypass. The C8-modified dGuo (X^7) and its complementary dCyd (C^{18}) are displaced toward the major groove in both duplexes. However, the complementary Cyt opposite the C8-Gua-cIQ is intra-helical, whereas it is completely displaced into the major grove when opposite the C8-Gua-IQ adduct.

Conclusions

2-Amino-3-methylimidazo[4,5-*f*]naphthelene, an analogue of the dietary mutagen IQ which has not yet been identified in cooked meats, is ~10^5 less effective at inducing two-base frameshift mutations in *Salmonella typhimurium* tester strain TA98 than IQ. Our data collectively suggests that the dramatically reduced mutagenicity of cIQ is due to differences in replication of the C8-dGuo-cIQ adduct, which was found to be a strong block to pol II^{-} and other polymerases when incorporated in the frameshift prone position of the *NarI* sequence. *E. coli* pol II is responsible for two-base frameshifts induced the C8-dGuo-AAF adduct in CG-dinucleotide repeat sequence, whereas bypass by pol IV and V largely resulted

in base-pair substitution and error-free bypass, respectively. Assuming the same polymerase-specific replication outcomes, our results suggest that the inability of pol II to bypass the C8-dGuo-cIQ lesion would require translesion synthesis by one of the other SOS polymerases resulting in a much lower frequency of two-base deletions and accounts for the lower activity of cIQ in Ames tester strain TA98.

Supplementary Material

Refer to Web version on PubMed Central for supplementary material.

Acknowledgments

The National Institutes of Health supported this work through research grants R01 CA122320 (R.J.T), R01 CA55678 (M.P.S.), R01 ES010375 (F.P.G.), and R01 ES016561 (C.J.R.), and center grant P30 ES000267 (M.P.S., C.J.R., and F.P.G). J.S.S. and C.A.G. were supported by pre-doctoral traineeship T32 ES07028 and T32 GM065086, respectively; G.C. was supported by a fellowship from Merck Research Laboratories. NIH Grant S10 RR-05805, the Vanderbilt Center in Molecular Toxicology, and Vanderbilt University provided funding for the NMR spectrometers.

References

(1). Turesky RJ. Formation and biochemistry of carcinogenic heterocyclic aromatic amines in cooked meats. Toxicol. Lett. 2007; 168:219–227. [PubMed: 17174486]

(2). Nagao, M.; Sugimura, T., editors. Food Borne Carcinogens: Heterocyclic Amines. J. Wiley & Sons; New York: 2000.

(3). Turesky RJ, Vouros P. Formation and analysis of heterocyclic aromatic amine-DNA adducts in vitro and in vivo. J. Chromatogr. B. 2004; 802:155–166.

(4). Schut HA, Snyderwine EG. DNA adducts of heterocyclic amine food mutagens: Implications for mutagenesis and carcinogenesis. Carcinogenesis. 1999; 20:353–368. [PubMed: 10190547]

(5). Turesky RJ, Markovic J. DNA adduct formation of the food carcinogen 2-amino-3-methylimidazo[4,5-*f*]quinoline at the C-8 and N^2 atoms of guanine. Chem. Res. Toxicol. 1994; 7:752–761. [PubMed: 7696529]

(6). Sugimura T. Overview of carcinogenic heterocyclic amines. Mutat. Res. 1997; 376:211–219. [PubMed: 9202758]

(7). Kaiser G, Harnasch D, King MT, Wild D. Chemical structure and mutagenic activity of aminoimidazoquinolines and aminonaphthimidazoles related to 2-amino-3-methylimidazo[4,5-*f*]quinoline. Chem. Biol. Interact. 1986; 57:97–106. [PubMed: 3512112]

(8). Vikse R, Klungsøyr L, Grivas S. Mutagenic activity of three synthetic isomers of the food carcinogen 2-amino-3-methylimidazo[4,5-*f*]quinoline (IQ) in the Ames test. Mutat. Res. 1993; 319:273–278. [PubMed: 7504200]

(9). Turesky RJ, Taylor J, Schnackenberg L, Freeman JP, Holland RD. Quantitation of carcinogenic heterocyclic aromatic amines and detection of novel heterocyclic aromatic amines in cooked meats and grill scrapings by HPLC/ESI-MS. J. Agric. Food Chem. 2005; 53:3248–3258. [PubMed: 15826085]

(10). Snyderwine EG, Welti DH, Fay LB, Würzner HP, Turesky RJ. Metabolism of the food mutagen 2-amino-3-methylimidazo[4,5-*f*]quinoline in nonhuman primates undergoing carcinogen bioassay. Chem. Res. Toxicol. 1992; 5:843–851. [PubMed: 1489936]

(11). Lakshmi VM, Hsu FF, Zenser TV. N-Demethylation is a major route of 2-amino-3-methylimidazo[4,5-*f*]quinoline metabolism in mouse. Drug Metab. Dispos. 2008; 36:1143–1152. [PubMed: 18356269]

(12). Kim D, Guengerich FP. Selection on human cytochrome P450 1A2 mutants with enhanced catalytic activity for heterocyclic amine *N*-hydroxylation. Biochemistry. 2004; 43:981–988. [PubMed: 14744142]

(13). Kadlubar FF, Miller JA, Miller EC. Hepatic metabolism of *N*-hydroxy-*N*-methyl-4-aminoazobenzene and other *N*-hydroxy arylamines to reactive sulfuric acid esters. Cancer Res. 1976; 36:2350–2359. [PubMed: 819129]

(14). Elmquist CE, Stover JS, Wang Z, Rizzo CJ. Site-specific synthesis and properties of oligonucleotides containing C8-deoxyguanosine adducts of the dietary mutagen IQ. J. Am. Chem. Soc. 2004; 126:11189–11201. [PubMed: 15355100]

(15). Cavaluzzi MJ, Borer PN. Revised UV extinction coefficients for nucleoside-5′-monophosphates and unpaired DNA and RNA. Nucleic Acids Res. 2004; 32:e13. [PubMed: 14722228]

(16). Wang F, De Muro NE, Elmquist CE, Stover JS, Rizzo CJ, Stone MP. Base-displaced intercalated structure of the food mutagen 2-amino-3-methylimidazo[4,5-*f*]quinoline (IQ) in the recognition sequence of the *Nar*I restriction enzyme, a hotspot for −2 bp deletions. J. Am. Chem. Soc. 2006; 128:10085–10095. [PubMed: 16881637]

(17). Brunger, AT. X-PLOR. Version 3.1. A system for X-ray crystallography and NMR. Yale University Press; New Haven, CT: 1992.

(18). Nilsson L, Karplus M. Empirical energy functions for energy minimization and dynamics of nucleic acids. J. Comput. Chem. 1986; 7:591–616.

(19). Stover JS, Chowdhury G, Zang H, Guengerich FP, Rizzo CJ. Translesion synthesis past the C8- and N^2-deoxyguanosine adducts of the dietary mutagen 2-amino-3-methylimidazo[4,5-*f*]quinoline in the *Nar*I recognition sequence by prokaryotic DNA polymerases. Chem. Res. Toxicol. 2006; 19:1506–1517. [PubMed: 17112239]

(20). Lowe LG, Guengerich FP. Steady-state and pre-steady-state kinetic analysis of dNTP insertion opposite 8-oxo-7,8-dihydroguanine by *Escherichia coli* polymerases I exo$^-$ and II exo$^-$. Biochemistry. 1996; 35:9840–9849. [PubMed: 8703958]

(21). Zang H, Goodenough AK, Choi JY, Irimia A, Loukachevitch LV, Kozekov ID, Angel KC, Rizzo CJ, Egli M, Guengerich FP. DNA adduct bypass polymerization by *Sulfolobus solfataricus* DNA polymerase Dpo4: Analysis and crystal structures of multiple base pair substitution and frameshift products with the adduct 1,N^2-ethenoguanine. J. Biol. Chem. 2005; 280:29750–29764. [PubMed: 15965231]

(22). Fay LB, Turesky RJ. Electron impact and fast atom bombardment mass spectrometric analysis of the food-borne carcinogens 2-amino-3-methylimidazo[4,5-*f*]quinoline, 2-amino-3,8-dimethylimidazo[4,5-*f*]quinoxaline and their metabolites. Biol. Mass Spectrom. 1992; 21:463–469. [PubMed: 1420382]

(23). Luks HJ, Spratt TE, Vavrek MT, Roland SF, Weisburger JH. Identification of sulfate and glucuronic acid conjugates of the 5-hydroxy derivative as major metabolites of 2-amino-3-methylimidazo[4,5-*f*]quinoline in rats. Cancer Res. 1989; 49:4407–4411. [PubMed: 2743329]

(24). Alexander J, Holme JA, Wallin H, Becher G. Characterisation of metabolites of the food mutagens 2-amino-3-methylimidazo[4,5-*f*]quinoline and 2-amino-3,4-dimethylimidazo[4,5-*f*]quinoline formed after incubation with isolated rat liver cells. Chem. Biol. Interact. 1989; 72:125–142. [PubMed: 2510946]

(25). Turesky RJ, Guengerich FP, Guillouzo A, Langouët S. Metabolism of heterocyclic aromatic amines by human hepatocytes and cytochrome P450 1A2. Mutat. Res. 2002; 506-507:187–195. [PubMed: 12351158]

(26). Zhou H, Josephy PD, Kim D, Guengerich FP. Functional characterization of four allelic variants of human cytochrome P450 1A2. Arch. Biochem. Biophys. 2004; 422:23–30. [PubMed: 14725854]

(27). Gangl ET, Turesky RJ, Vouros P. Determination of in vitro- and in vivo-formed DNA adducts of 2-amino-3-methylimidazo[4,5-*f*]quinoline by capillary liquid chromatography/microelectrospray mass spectrometry. Chem. Res. Toxicol. 1999; 12:1019–1027. [PubMed: 10525280]

(28). Jamin EL, Arquier D, Canlet C, Rathahao E, Tulliez J, Debrauwer L. New insights in the formation of deoxynucleoside adducts with the heterocyclic aromatic amines PhIP and IQ by means of ion trap MS^n and accurate mass measurement of fragment ions. J. Am. Soc. Mass Spectro. 2007; 18:2107–2118.

(29). Malmberg EW, Hamilton CS. The synthesis of 2- and 3-substituted naphth[1,2]imidazoles. J. Am. Chem. Soc. 1948; 70:2415–2417.

(30). Bonala R, Torres MC, Iden CR, Johnson F. Synthesis of the PhIP adduct of 2′-deoxyguanosine and its incorporation into oligomeric DNA. Chem. Res. Toxicol. 2006; 19:734–738. [PubMed: 16780350]

(31). Takamura-Enya T, Ishikawa S, Mochizuki M, Wakabayashi K. Chemical synthesis of 2′-deoxyguanosine-C8 adducts with heterocyclic amines: An application to synthesis of oligonucleotides site-specifically adducted with 2-amino-1-methyl-6-phenylimidazo[4,5-*b*]pyridine. Chem. Res. Toxicol. 2006; 19:770–778. [PubMed: 16780355]

(32). Fuchs RP, Schwartz N, Daune MP. Hot spots of frameshift mutations induced by the ultimate carcinogen *N*-acetoxy-*N*-2-acetylaminofluorene. Nature. 1981; 294:657–659. [PubMed: 7031481]

(33). Fuchs RP, Fujii S. Translesion synthesis in *Escherichia coli*: Lessons from the *Nar*I mutation hot spot. DNA Repair. 2007; 6:1032–1041. [PubMed: 17403618]

(34). Elmquist CE, Wang F, Stover JS, Stone MP, Rizzo CJ. Conformational Differences of the C8-deoxyguanosine Adduct of the Dietary Mutagen 2-amino-3-methylimidazo[4,5-*f*]quinoline (IQ) within the *Nar*I recognition sequence. Chem. Res. Toxicol. 2007; 20:445–454. [PubMed: 17311423]

(35). Liang F, Meneni S, Cho BP. Induced circular dichroism characteristics as conformational probles for carcinogenic aminoflourene-DNA adducts. Chem. Res. Toxicol. 2006; 19:1040–1043. [PubMed: 16918242]

(36). Turesky RJ, Lang NP, Butler MA, Teitel CH, Kadlubar FF. Metabolic activation of carcinogenic heterocyclic aromatic amines by human liver and colon. Carcinogenesis. 1991; 12:1839–1845. [PubMed: 1934265]

(37). Turesky RJ, Constable A, Richoz J, Varga N, Markovic J, Martin MV, Guengerich FP. Activation of heterocyclic aromatic amines by rat and human liver microsomes and by purified rat and human cytochrome P450 1A2. Chem. Res. Toxicol. 1998; 11:925–936. [PubMed: 9705755]

(38). Kanazawa K, Ashida H, Danno G. Comparison in metabolic activity of cytochrome P450 1A1 on heterocyclic amines between human and rat. J. Agric. Food Chem. 1999; 47:4956–4961. [PubMed: 10606558]

(39). Novak M, Rajagopal S, Xu L, Kazerani S, Toth K, Brooks M, Nguyen T. Chemistry of carcinogenic and mutagenic metabolites of heterocyclic aromatic amines. J. Phys. Org. Chem. 2004; 17:615–624.

(40). Hoffmann GR, Fuchs RP. Mechanisms of frameshift mutations: Insight from aromatic amines. Chem. Res. Toxicol. 1997; 10:347–359. [PubMed: 9114969]

(41). Becherel OJ, Fuchs RP. Mechanism of DNA polymerase II-mediated frameshift mutagenesis. Proc. Natl. Acad. Sci. U.S.A. 2001; 98:8566–8571. [PubMed: 11447256]

(42). Fujii S, Fuchs RP. Interplay among replicative and specialized DNA polymerases determines failure or success of translesion synthesis pathways. J. Mol. Biol. 2007; 372:883–893. [PubMed: 17707403]

(43). Gill JP, Romano LJ. Mechanism for *N*-acetyl-2-aminofluorene-induced frameshift mutagenesis by *Escherichia coli* DNA polymerase I (Klenow fragment). Biochemistry. 2005; 44:15387–15395. [PubMed: 16285743]

(44). Tan X, Suzuki N, Grollman AP, Shibutani S. Mutagenic events in *Escherichia coli* and mammalian cells generated in response to acetylaminofluorene-derived DNA adducts positioned in the *Nar*I restriction enzyme site. Biochemistry. 2002; 41:14255–14262. [PubMed: 12450390]

(45). Choi J-Y, Stover JS, Angel KC, Chowdhury G, Rizzo CJ, Guengerich FP. Biochemical basis of genotoxicity of heterocyclic arylamine food mutagens: Human DNA polymerase η selectively produces a two-base deletion in copying the N^2-guanyl adduct of 2-amino-3-methylimidazo[4,5-*f*]quinoline but not the C8-adduct at the *Nar*I G3 site. J. Biol. Chem. 2006; 281:25297–25306. [PubMed: 16835218]

(46). Mao B, Hingerty BE, Broyde S, Patel DJ. Solution structure of the aminofluorene [AF]-intercalated conformer of the *syn*-[AF]-C^8-dG adduct opposite dC in a DNA duplex. Biochemistry. 1998; 37:81–94. [PubMed: 9425028]

(47). Mao B, Hingerty BE, Broyde S, Patel DJ. Solution structure of the aminofluorene [AF]-external conformer of the *anti*-[AF]-C^8-dG adduct opposite dC in a DNA duplex. Biochemistry. 1998; 37:95–106. [PubMed: 9425029]

(48). Mao B, Gorin A, Gu Z, Hingerty BE, Broyde S, Patel DJ. Solution structure of the aminofluorene-intercalated conformer of the *syn* [AF]-C^8-dG adduct opposite a −2 deletion site in the *Nar*I hot spot sequence context. Biochemistry. 1997; 36:14479–14490. [PubMed: 9398167]

(49). Patel DJ, Mao B, Gu Z, Hingerty BE, Gorin A, Basu AK, Broyde S. Nuclear magnetic resonance solution structures of covalent aromatic amine-DNA adducts and their mutagenic relevance. Chem. Res. Toxicol. 1998; 11:391–407. [PubMed: 9585469]

(50). Wang F, Elmquist CE, Stover JS, Rizzo CJ, Stone MP. DNA sequence modulates the conformation of the food mutagen 2-amino-3-methylimidazo[4,5-*f*]quinoline in the recognition sequence of the *Nar*I restriction enzyme. Biochemistry. 2007; 46:8498–8546. [PubMed: 17602664]

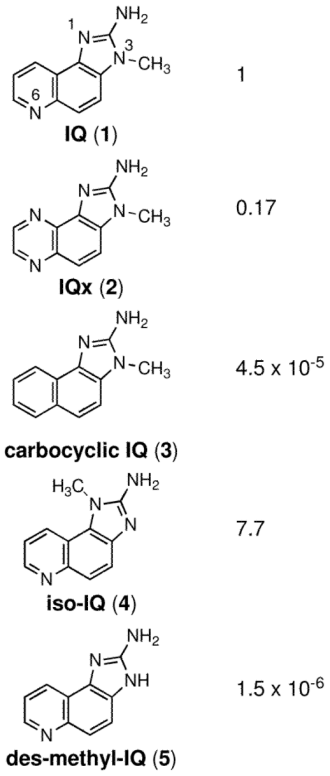

Figure 1.
Structure and relative mutagenicity (revertants/μg) of IQ, IQx and analogues in Ames tester strain TA98

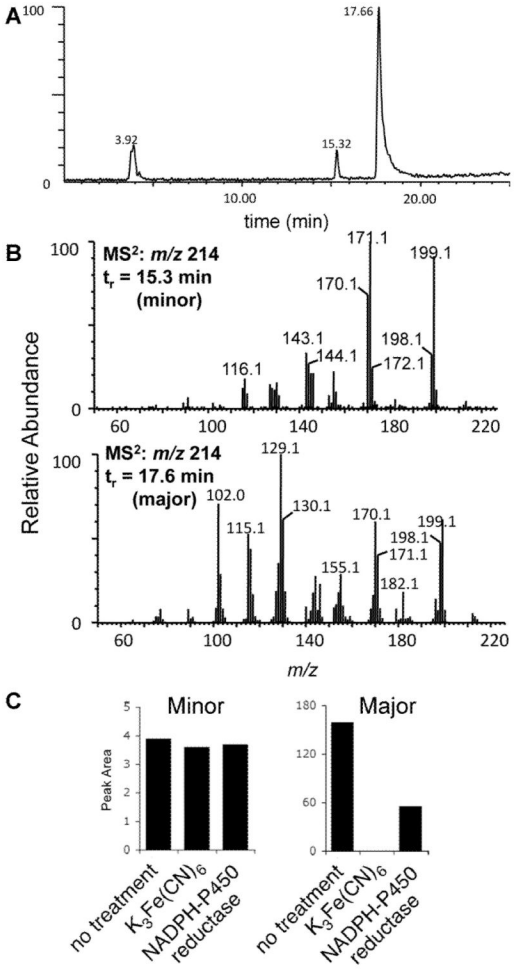

Figure 2.

Microsomal oxidation products of cIQ. **A.** ESI-LC-MS chromatogram (*m/z* 214) of the oxidation of cIQ with rat liver microsomes. **B.** Mass spectrum of the major (top) and minor (bottom) oxidation product of cIQ **C.** Relative peak areas of the microsomal oxidation products of cIQ remaining after treatment with $K_3Fe(CN)_6$ or NADPH-P450 reductase.

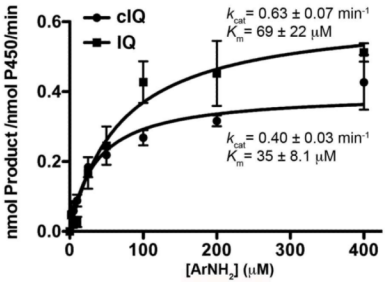

Figure 3.

Rates of microsomal oxidation of IQ and cIQ. A solution of rat liver microsomes (0.4 μM of P450), potassium phosphate buffer (100 mM, pH 7.0), NADPH-generating system and varying concentration of IQ or cIQ (0-200 μM) in a total volume of 500 μL were incubated for 10 min at 37 °C.

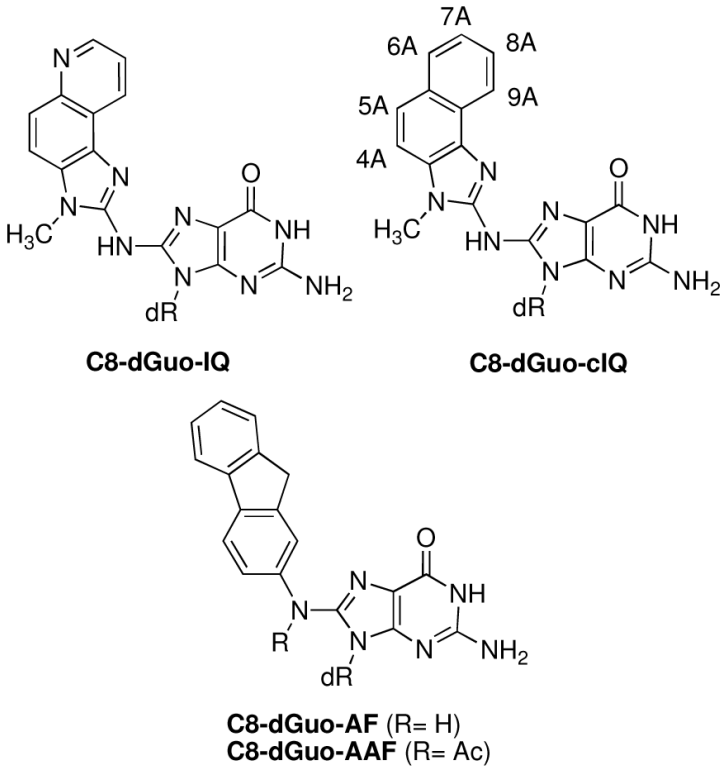

Figure 4.

C8-dGuo adducts of 2-amino-3-methylimidazo[4,5-*f*]quinoline (IQ), 2-amino-3-methylimidazo[4,5-*f*]naphthelene (cIQ), 2-aminofluorene (AF), and *N*-acetyl-2-aminoflourene (AAF)

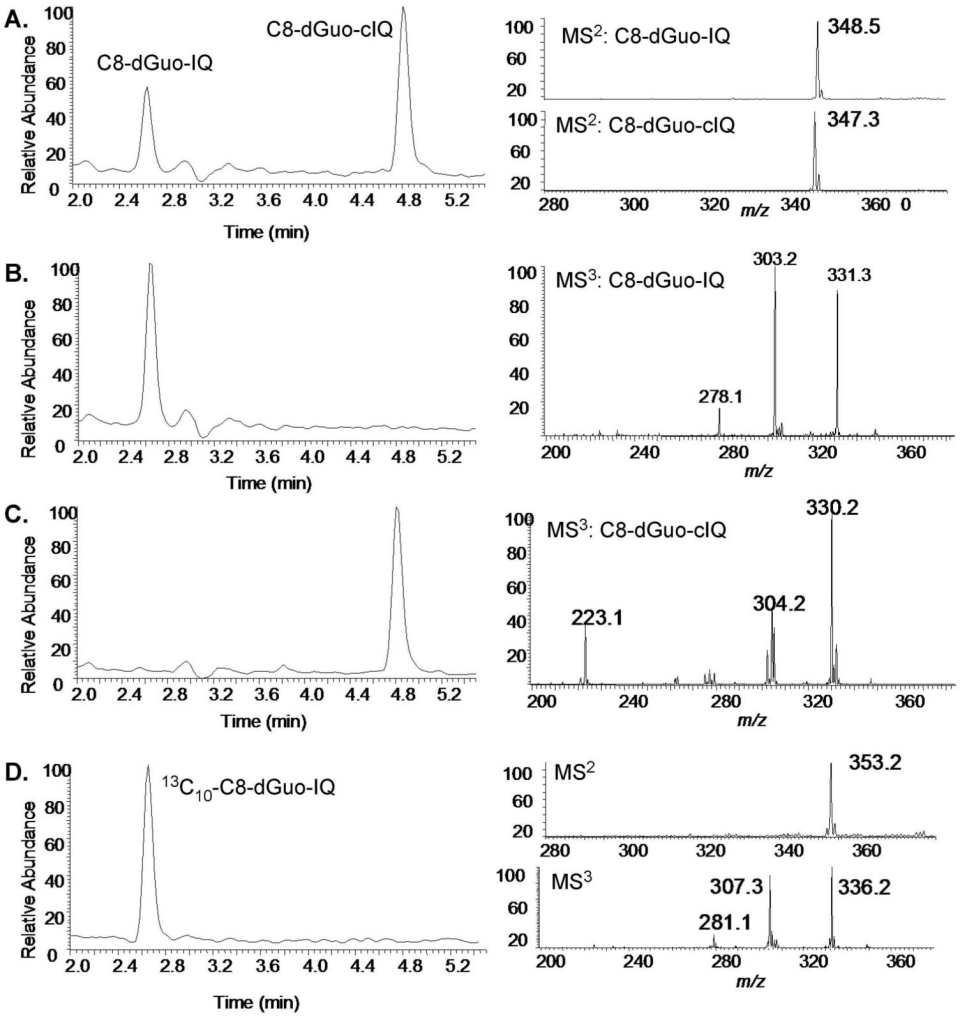

Figure 5.

UPLC-ESI/MS/MS^n analysis of the reaction of activated IQ and cIQ with calf thymus DNA. **A.** UPLC-ESI/MS/MS chromatograph of the C8-dGuo-IQ (t_r = 2.6 min) and C8-dGuo-cIQ (t_r = 4.8 min) adducts formed from the activation of IQ and cIQ by rat liver microsomes and acetic anhydride followed by the modification of calf thymus DNA. MS/MS spectra (M+H −dR) of the two adducts are shown on the right. **B.** UPLC-ESI-MS/MS^3 chromatogram of the reconstructed ion profile at *m/z* 331 of the C8-dGuo-IQ adducts (left) and its MS^3 product ion spectrum (464 → 348 → 331)(right). **C.** UPLC-ESI-MS/MS^3 chromatogram of the reconstructed ion profile at *m/z* 347 (left) of the C8-dGuo-cIQ adducts and its MS^3 product ion spectrum (*m/z* 463 → 347 → 330) (right). **D.** UPLC-ESI-MS/MS^3 chromatogram of the reconstructed ion profile at *m/z* 473 (left) of the $^{13}C_{10}$-C8-dGuo-IQ standard and its MS/MS and MS^3 product ion spectra (right).

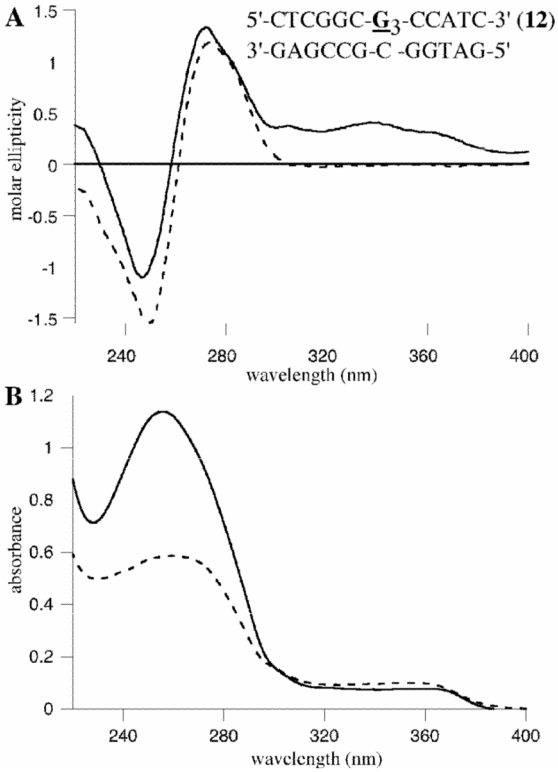

Figure 6.

A. CD spectra of duplex of **12** containing the C8-dGuo-cIQ adduct (———) and the unmodified oligonucleotide (-------). **B.** UV spectra of the C8-dGuo-cIQ containing oligonucleotide **12** in single strand (-------) and duplex (———).

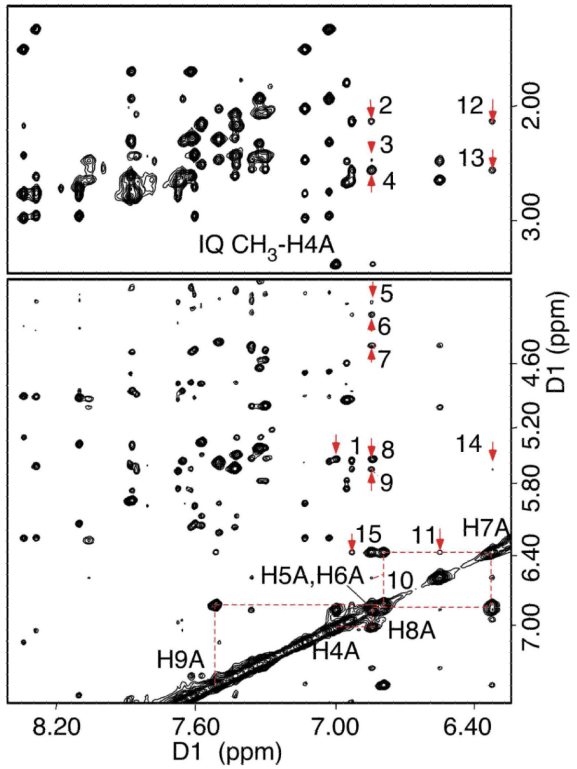

Figure 7.

Tile plots showing NOE cross-peaks between non-exchangeable protons of DNA and cIQ protons in duplex DNA. 1, G^{19} H1′→cIQ H4A; 2, G^{17} H2′→cIQ H6A; 3, C^{18} H2′→cIQ H6A; 4, G^{17} H2″→cIQ H6A; 5, G^{19} H5″→ cIQ H5A; 6, G^{19} H5′→ cIQ H5A; 7, G^{19} H4′→ cIQ H5A; 8, G^{19} H1′→ cIQ H5A; 9, G^{17} H1′→ cIQ H5A; 10, C^{18} H1′→ cIQ H5A; 11, C^{18} H1′→ cIQ H7A; 12, G^{17} H2′→cIQ H7A; 13, G^{17} H2″→cIQ H7A; 14, G^{17} H1′→cIQ H7A; 15, G^{17} H8→cIQ H7A.

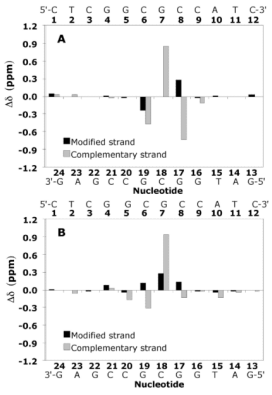

Figure 8.

Chemical shift changes of (**A**) aromatic protons H6/H8 and (**B**) anomeric H1′ protons of the C8-dGuo-cIQ modified duplex in the *Nar*I sequence, relative to the unmodified duplex, where $\Delta\delta = [\delta_{modified} - \delta_{unmodified}]$ (ppm).

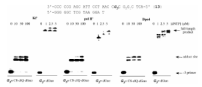

Figure 9.
Bypass and extension assay of the C8-dGuo-cIQ adduct by Kf⁻, pol II⁻, and Dpo4.

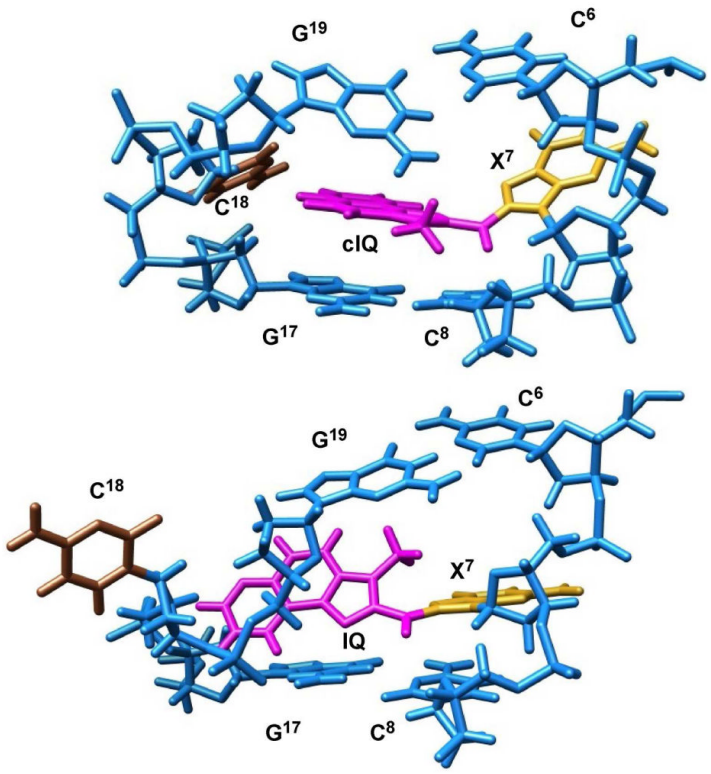

Figure 10.

The average refined structures of the C8-dGuo-cIQ (top) and C8-dGuo-IQ (bottom) adducts at the G_3-position of the *Nar*I recognition sequence and the flanking base pairs situated (**12**), looking into the minor groove. The cIQ and IQ adducts are in magenta, the modified Gua (X^7) is in gold, and the complementary Cyd (C^{18}) in brown. See Figure 8 for full sequence and residue numbering.

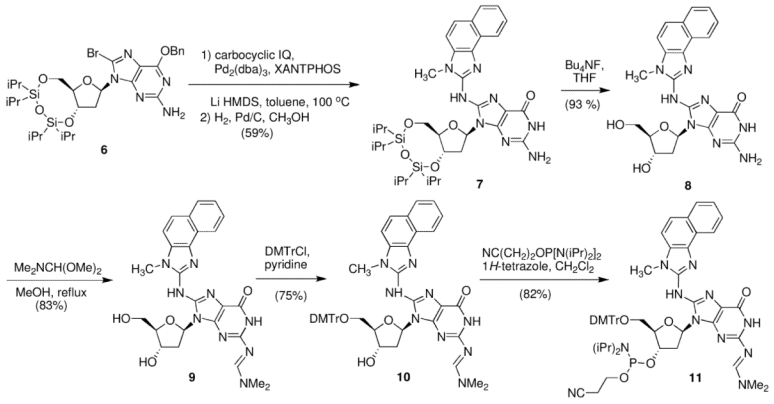

Scheme 1.

Table 1

Adducts levels of C8-dGuo-IQ and C8-dGuo-cIQ (pmols/mg of DNA) detected by LC-ESI-MS/MS after activation of IQ and cIQ and reaction with calf thymus DNA obtained

adduct	acetic anhydride	acetylCoA / NAT
C8-dGuo-IQ	2.1 (60 adducts / 10^8 bases)	0.12 (4 adducts / 10^8 bases)
C8-dGuo-cIQ	4.4 (150 adducts / 10^8 bases)	0.35 (12 adducts / 10^8 bases)

Table 2

Chemical shifts (δ) of the IQ and cIQ protons for the nucleoside and in oligonucleotide **12** (34)

proton	C8-dGuo-IQ [a]	12 (G3= C8-dGuo-IQ) [b]	C8-dGuo-cIQ [a]	12 (G3= C8-dGuo-cIQ) [b]
H4A	7.39	7.27	7.72	7.03
H5A	7.28	7.11	7.67	6.88
H6A	-------	-------	7.99	6.88
H7A	8.34	8.07	7.44	6.39
H8A	7.10	6.70	7.62	6.84
H9A	8.20	7.80	8.14	7.53

[a] recorded in DMSO-d_6 at 400 MHz

[b] recorded in 10 mM, pH 7.0 phosphate at 800 MHz